3610–3620 *Nucleic Acids Research, 1999, Vol. 27, No. 17*

Nucleotide excision repair in a constitutive and inducible gene of a yeast minichromosome in intact cells

Shisheng Li[1], Magdalena Livingstone-Zatchej[2], Ranjan Gupta[1,3], Maria Meijer[1], Fritz Thoma[2] and Michael J. Smerdon[1,*]

[1]Department of Biochemistry and Biophysics, Washington State University, Pullman, WA 99164-4660, USA, [2]Institut für Zellbiologie, ETH-Hönggerberg, CH-8093 Zürich, Switzerland and [3]National Center for Biotechnology Information, National Library of Medicine, National Institutes of Health, Bethesda, MD 20894, USA

Received March 12, 1999; Revised and Accepted July 6, 1999

ABSTRACT

Repair of UV-induced cyclobutane pyrimidine dimers (CPDs) was measured in a yeast minichromosome, having a galactose-inducible *GAL1:URA3* fusion gene, a constitutively expressed *HIS3* gene and varied regions of chromatin structure. Transcription of *GAL1:URA3* increased >150-fold, while *HIS3* expression decreased <2-fold when cells were switched from glucose to galactose medium. Following galactose induction, four nucleosomes were displaced or rearranged in the *GAL3–GAL10* region. However, no change in nucleosome arrangement was observed in other regions of the minichromosome following induction, indicating that only a few plasmid molecules actively transcribe at any one time. Repair at 269 *cis-syn* CPD sites revealed moderate preferential repair of the transcribed strand of *GAL1:URA3* in galactose, consistent with transcription-coupled repair in a fraction of these genes. Many sites upstream of the transcription start site in the transcribed strand were also repaired faster upon induction. There is remarkable repair heterogeneity in the *HIS3* gene and preferential repair is seen only in a short sequence immediately downstream of the transcription start site. Finally, a mild correlation of repair heterogeneity with nucleosome positions was observed in the transcribed strand of the inactive *GAL1:URA3* gene and this correlation was abolished upon galactose induction.

INTRODUCTION

DNA repair is an important defense mechanism against phenotypic changes and mutations in virtually all cells (1). Such changes can be an important etiological factor in cell survival and cancer (see for example 2,3). For example, DNA lesions may alter the expression of specific genes required for establishing the neoplastic phenotype.

Most types of DNA damage that cause helical distortions in the DNA molecule are repaired by the nucleotide excision repair (NER) pathway (1). Examples of these types of lesions are *cis-syn* cyclobutane pyrimidine dimers (CPDs), induced by UV radiation, and a number of different adducts formed by polyaromatic hydrocarbons. NER in eukaryotic cells is a complex biochemical process involving multiple gene products. At least nine and 17 proteins are indispensible for this process in *Saccharomyces cerevisiae* and mammalian cells, respectively (1). This pathway involves single-strand incisions 3' and 5' of the damaged base (or bases), excision of a 24–32 base oligonucleotide by a DNA helicase and gap repair synthesis and resealing by DNA polymerase and DNA ligase, respectively (4,5). Furthermore, NER is more rapid in the transcribed strand (TS) of many active genes (referred to as transcription-coupled repair) than in the non-transcribed strand (NTS) or in the genome overall (1,5,6).

Studies using yeast minchromosomes have shown that transcription-coupled repair also occurs in the active genes of yeast plasmids (7,8) and the rate of repair may correlate with both the rate of transcription and the stablility of nucleosomes (9,10). More recently, Wellinger and Thoma (11) showed that in the NTS of the *URA3* gene of the yeast minichromosome YRpTRURAP rapid repair of CPDs occurs in linker DNA and towards the 5'-end of a positioned nucleosome, while slow repair occurs in the internal protected region of the nucleosome core. Recently this was also observed in the genomic *URA3* gene (12). This raises the possibility that repair of the NTS of active genes can be modulated by nucleosome folding and this modulation is superseded by transcription elongation in the transcribed strand.

Several questions arise from these studies. For example, is the correlation between repair rates and nucleosome positions a general phenomenon or restricted to the NTS of the *URA3* gene? Moreover, is there any difference in transcription–repair coupling between an inducible gene and a constitutive gene in yeast minichromosomes? To address these questions, we have

*To whom correspondence should be addressed. Tel: +1 509 335 6853; Fax: +1 509 335 9688; Email: smerdon@mail.wsu.edu
Present address:
Maria Meijer, Cancer Biology Group, Department of Biochemistry and Molecular Biology, University of Calgary Medical Centre, 3330 Hospital Drive NW, Calgary, Alberta T2N 4N1, Canada

The authors wish it to be known that, in their opinion, the first three authors should be regarded as Joint First Authors

studied repair of CPDs induced by UV radiation in a 4.3 kb autonomously replicating plasmid (YRpSO1) in intact yeast cells. This minichromosome contains a constitutively expressed *HIS3* gene, a galactose-inducible *GAL1:URA3* fusion gene, an autonomous replication region (*ARS1*), the upstream region of the *GAL3* gene and 22 positioned nucleosomes.

MATERIALS AND METHODS

Plasmid and yeast strains

Bacterial sequences were removed from plasmid pYRpSO1 (13) by cutting with *Eco*RI and self-ligating the yeast DNA. The resulting plasmid YRpSO1 (Fig. 1) consists of the following elements: the *GAL1-10* promoter as an *Eco*RI–*Bam*HI fragment from pBM150 (kindly provided by Dr M. Johnston) (14) fused to the coding region of the *URA3* gene (a 950 bp *Pst*I–*Hin*dIII fragment; 15,16), with the *GAL1* promoter element facing the *URA3* sequence; the *Hin*dIII–*Eco*RI fragment from pBRAT2 (17) containing the *TRP1–ARS1* sequences and upstream elements of the *GAL3* gene (18,29); the 1765 bp *Bam*HI fragment containing the chromosomal *PET56–HIS3–DED1* sequence (19) inserted in the *GAL3* sequence. Strain RGY1 was made by transforming *S.cerevisiae* strain Y452 (MATα *ura3-52 his3-1 leu2-3 leu2-112 cir°*), obtained from Dr Louise Prakash (University of Texas, Galveston, TX), with YRpSO1. Transformations were done following a modified protocol of Ito *et al*. (20) using single-stranded calf thymus DNA as carrier (21) and selecting on plates containing no histidine.

Transcription of YRpSO1

Total RNA from yeast cells was isolated following a modified protocol of Ausubel *et al*. (22) and analyzed by northern blot as described previously (9). RNA was transferred to nylon membranes (e.g. Hybond N^+; Amersham) in the presence of 10× SSC (1.5 M NaCl, 0.15 M sodium citrate, pH 7.0). The membranes were baked at 80°C for 2 h and treated with a hot solution of 0.1× SSC, 0.1% SDS just before hybridization. Hybridizations were carried out at 42°C in the presence of 50% (v/v) formamide, 7% (w/v) SDS, 0.25 M NaH_2PO_4, pH 7.0, 0.25 M NaCl and 1 mM EDTA. For analysis of transcription from the *URA3* and *HIS3* genes specifically, fragments of these genes were inserted into bidirectional promoter vectors. Probes for the *URA3* region were generated from pBSURA3/503 containing a 503 bp *Stu*I–*Hin*dIII fragment of the *URA3* gene, using T3 or T7 RNA polymerase as previously described (9). Likewise, T3/T7 RNA probes for the *HIS3* region were generated from pBSFT94 (a construct containing an internal 187 bp *Hin*dIII fragment from the *HIS3* gene introduced in tandem repeat at the *Hin*dIII site of the Bluescript KS^+ vector) linearized with *Eco*RI or *Sal*I, respectively. *In vitro* transcription reactions for making strand-specific RNA probes were performed in the presence of [γ-^{32}P]UTP (800 Ci/mmol; NEN Life Science Products), using the Stratagene labeling kit according to the manufacturer's instructions.

For half-life analyses of *URA3* transcripts, log-phase cultures grown in galactose were collected and resuspended in water containing 2% glucose to shut off transcription from the *GAL1-10* promoter. The abundance of *URA3* transcript at various times after incubation in glucose solution was monitored by northern analysis using strand-specific RNA probes generated from pBSURA3/503 (see above). After hybridization, membranes were exposed to phosphorimager screens and visualized on a Molecular Dynamics (model 445-P90) PhosphorImager (Sunnyvale, CA). Photographic negatives of ethidium bromide-stained gels (obtained prior to transfer) were scanned with a laser densitometer (Molecular Dynamics model PDSI-P90) and analyzed with ImageQuaNT (Molecular Dynamics) software.

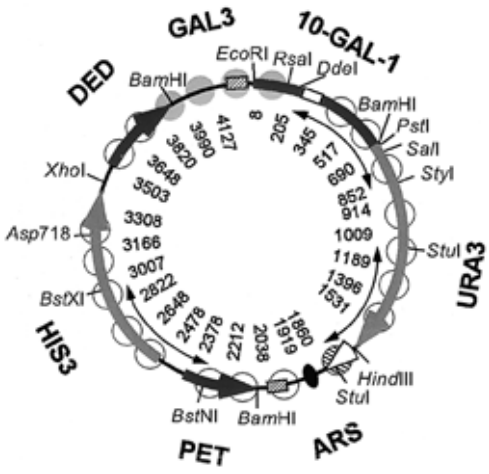

Figure 1. Schematic drawing of YRpSO1. DNA elements are indicated on the large circle. Small circles denote approximate nucleosome positions. Shaded circles in the *GAL3–GAL10* region denote nucleosomes that are destabilized or rearranged in galactose cultures. The hatched circle downstream of *URA3* indicates space for a nucleosome, although the footprint was unclear. The open box in the *GAL1-10* region denotes the UAS_g of the *GAL1* and *GAL10* genes. The two hatched boxes separated by the *PET56–HIS3–DED1* sequences denote UAS_g1 and UAS_g2 of the *GAL3* gene, respectively. The small solid ellipse demarcates the *ARS1* consensus sequence (A-element). The open arrowhead dowstream of *URA3* denotes the 3'-end of the *TRP1* gene. The inner, double-headed arrows indicate the fragments used to analyze repair of CPDs at specific sites and the numbers denote the nt positions (clockwise from the unique *Eco*RI site of YRpSO1) of strong micrococcal nuclease cut sites in chromatin.

Chromatin analysis of YRpSO1

Yeast cells were grown in 3 × 1 l of SD or SG medium (minimal medium containing glucose or galactose, respectively) at 30°C to an optical density of 0.6–0.7 at 600 nm. Preparation of chromatin and deproteinized control DNA, digestion with micrococcal nuclease and mapping of the cutting sites by indirect end-labeling were done as described previously (23), with the following modifications: Zymolyase 100T (ICN Pharmaceuticals) and a Sephacryl S300 column (Pharmacia) were used. Micrococcal nuclease (Sigma) was used at 0.013–1.67 U/ml of SD chromatin and at 0.017–0.5 U/ml of SG chromatin. Mapping was done from the *Asp*718 and *Xho*I sites using a labeled *Asp*718–*Xho*I fragment of the *HIS3* gene as a probe, from the *Eco*RI site using a labeled *Eco*RI–*Rsa*I fragment of the *GAL1-10* promoter or from the *Sal*I site using a labeled *Rsa*I–*Bam*HI fragment of the *GAL1-10* promoter (Fig. 1). Probes were made using a random priming kit (Pharmacia). Band sizes on autoradiographs were analyzed using a DIGIGEL program (DNAStar).

UV irradiation and DNA repair incubation

RGY1 cells were grown at 30°C in SD or SG medium to late log phase ($OD_{600} \approx 1.0$). For UV irradiation, cells were washed once with ice-cold 2% glucose or 2% galactose and resuspended in the same solutions to give an OD_{600} value of 1.0. Cells were irradiated in a dark room with 50 J/m^2 of 254 nm UV light. One-tenth volume of a solution containing 10% yeast extract and 20% peptone was then added to the irradiated cultures. After 0, 1, 2 and 4 h of repair incubation at 30°C, an aliquot was removed and stored on ice. Supercoiled YRpSO1 plasmid DNA was isolated following preparation of spheroplasts with Zymolyase 100T (ICN Pharmaceuticals) as described previously (24).

Analysis of CPD repair in whole plasmid DNA

Supercoiled YRpSO1 plasmid DNA, in TE (10 mM Tris, 1 mM EDTA, pH 8.0), was either untreated or treated with a vast excess of T4 endonuclease V (T4 endo V; a gift from Dr R. Stephen Lloyd, University of Texas, Galveston, TX) required to cut all CPD sites present. The T4 endo V-treated plasmid DNA was electrophoresed on neutral 1% agarose gels at 9.9 V/cm for 2–3 h in the presence of ethidium bromide (0.5 μg/ml). Gels were either photographed for direct quantitation from negatives or treated with 0.25 M HCl for 15 min (to depurinate DNA) and neutralized in 0.5 M NaOH, 1.5 M NaCl for 1 h before Southern blotting. The probe used for hybridization was generated from linearized YRpSO1 (see above). Membranes were exposed to preflashed X-ray film (Hyperfilm MPTM; Amersham) and an intensifying screen (22) at –80°C or to phosphorimager screens and visualized as described above. Photographic negatives of ethidium bromide-stained gels and autoradiograms were scanned with a laser densitometer (Molecular Dynamics model PDSI-P90) and analyzed using ImageQuaNT (Molecular Dynamics) software. Where necessary, 'nested peaks' were deconvoluted using the program PeakFit 4.0 (SPSS Science) as previously described (see for example 25). The average level of CPDs per plasmid was obtained from the intensity of the uncut (Form I) plasmid, assuming a Poisson distribution of UV damaged fragments, as described (24).

Analysis of CPD repair at specific sites in three selected fragments of YRpSO1

To monitor repair of CPDs at nucleotide resolution, a biotinylated oligonucleotide (oligo) and streptavidin magnetic bead-facilitated end-labeling technique was used (25–27). Briefly, isolated plasmid DNA was cut with restriction enzyme(s) to release the specific fragments to be analyzed (Fig. 1, double headed arrows). *Dde*I and *Sty*I were used to release the 678 bp *GAL1–URA3* fragment, which contains the UAS_g, the promoter and a short 5' coding sequence of the *GAL1* gene and a segment of the 5' sequence of the fused *URA3* gene. *Stu*I was used to release the 717 bp *URA3*–3' fragment containing the 3' portion of the *URA3* gene and a 3' part of the *TPR1* gene (13). *Bst*NI and *Bst*XI was used to release the 659 bp *HIS3* fragment, which contains a short sequence of the *PET56* gene and the promoter and 5' coding region of the *HIS3* gene. The restricted DNA was incised at CPD sites by treatment with T4 endo V at 37°C for 1 h. To quantitatively measure CPD formation and repair at individual sites, we used an excess amount of T4 endo V to ensure that all CPD sites were incised by the enzyme (routinely checked with irradiated plasmid). The 3'-ends of one strand of the incised fragments were annealed to biotinylated oligos containing a sequence complementary to that end. The oligos used were: (i) for the *GAL1–URA3* fragment, 5'-biotin-GATACG-TTTTTTGCCTAAAAAAACCTTCTCTTTGGAA for labeling the TS of the *URA3* gene and 5'-biotin-GATACGTTTTTTGT-GGTACGAACATCCAATGAAGC for labeling the NTS of the *URA3* gene; (ii) for the *URA3*–3' fragment, 5'-biotin-GATACGTTTTTTCCTTTTGATGTTAGCAGAATTGTCATG for labeling the TS of the *URA3* gene and 5'-biotin-GAT-ACGTTTTTTCCTGCAGGCAAGTGCACAAA for labeling the NTS of the *URA3* gene; (iii) for the *HIS3* fragment, 5'-biotin-GATACGTTTTTTGGTATCGTTTGAACACGGCATTAGT for labeling the TS of the *HIS3* gene and 5'-biotin GAT-ACGTTTTTTCGCTCTGGAAAGTGCCTCATC for labeling the NTS of the *HIS3* gene. The annealed fragments were attached to streptavidin magnetic beads (Dynal) and labeled using [α-^{32}P]dATP (NEN Life Science Products) and Sequenase (Amersham). The labeled fragments were eluted and resolved on 20 × 60 cm sequencing gels. The top parts of gels containing no radioactive signals were cut off after electrophoresis and the gels were exposed to 35 × 43 cm phosphorimager screens (Molecular Dynamics). DNA damage levels at each repair time were quantified by integrating band intensities in gel lanes for different repair incubation times using ImagQuaNT (Molecular Dynamics) and PeakFit 4.0 (SPSS) software as described (25).

Sequence markers were generated from the fragments obtained by standard PCR reaction. The primers used for PCR were the same as the oligos used for end-labeling, except that the primers only contained the sequences complementary to the 3'-ends of one strand of the fragments of interest (without the 5' biotin and six arbitrary Ns and Ts). The PCR products were modified at specific bases and cleaved using a modification of the 'rapid' Maxam–Gilbert sequencing procedure (28) as described previously (25–27). The cleaved products were stored at –20°C and labeled at the same time as the (damage-specific) incised DNA fragments, using the identical procedure.

RESULTS

General features of YRpSO1

The YRpSO1 construct is a high copy number (~50 copies/cell), autonomously replicating yeast plasmid 4.3 kb in length (Fig. 1). It contains: (i) the *ARS1* origin of replication, flanked by the 3'-end of the *TRP1* gene and a portion of the upstream region of the *GAL3* gene (29); (ii) the *URA3* sequence fused to the divergent *GAL1* promoter; (iii) a constitutive *HIS3* gene serving as a selectable marker; (iv) the 5'-ends of the *PET56* and *DED1* genes of *S.cerevisiae*; (v) another portion of the *GAL3* upstream sequence placed between the *DED1* sequence and the *GAL1-10* promoter (13). Transcription of the *GAL1:URA3* gene is repressed in glucose and induced in galactose, while the *HIS3* gene is constitutively expressed in both glucose and galactose (see below). YRpSO1 has 22 nucleosomes (Fig. 1, small open and shaded circles) distributed in four nucleosomal regions, interrupted by four non-nucleosomal, nuclease-sensitive gaps (13; see below).

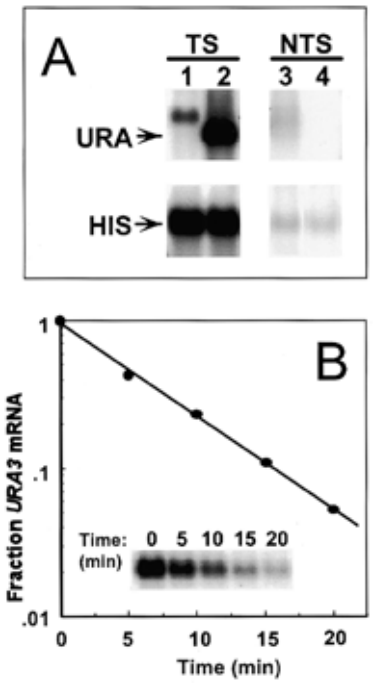

Figure 2. (**A**) RNA transcripts from YRpSO1. Total RNA was isolated from late log-phase RGY1 cells, grown in glucose (lanes 1 and 3) or galactose (lanes 2 and 4) medium and subjected to northern blot analysis using strand-specific riboprobes to the *URA3* or *HIS3* genes. (**B**) Decay of *URA3* mRNA. RGY1 cells were grown in galactose medium to late log phase, collected and resuspended in water plus 2% glucose at time 0. Total RNA was extracted at the indicated times and subjected to northern blot analysis (inset) using the URA3/NTS probe. The amount of *URA3* transcript in each lane was normalized to the amount of rRNA in that lane (to correct for loading variations) and divided by the value obtained for time 0. The half-life for the data shown is 4.5 min.

Transcription in YRpSO1

Expression of RNA from YRpSO1 was examined by northern blot analysis. Total RNA was isolated from log-phase cells grown in the presence of either glucose or galactose, separated by electrophoresis, blotted and hybridized with different strand-specific RNA probes (Materials and Methods). As shown in Figure 2A, the correct length of *URA3* mRNA is seen only in cells grown in galactose (lane 2, upper panel). Moreover, only a very weak signal is detected from the NTS of *URA3* in either glucose or galactose when autoradiograms are overexposed (lanes 3 and 4, respectively). In addition, a minor transcript is also expressed from the TS of *URA3* in glucose cultures (lane 1, upper panel), presumably representing a longer transcript of the gene made in a fraction of cells. Finally, as expected, the *HIS3* transcript is seen in both glucose- and galactose-grown cells from the TS of *HIS3* (lanes 1 and 2 of lower panel, respectively). Relative amounts of each transcript were obtained from scans of autoradiograms and loading differences between lanes were corrected to the levels of rRNA in each lane. Induction of *URA3* in galactose was >150-fold compared with cells grown in glucose [assuming a finite (non-zero) value for its expression in glucose], while expression of the *HIS3* gene decreased by <2-fold (10).

For comparison of the time course of *URA3* repair to the time course of transcription in galactose, the rate of synthesis of *URA3* mRNA was estimated from the rate of decay. At steady-state, the zero order rate of synthesis can be estimated from the first order rate of decay and the level of *URA3* mRNA (9,30). Following inhibition of *URA3* transcription by incubation in glucose, the half-life of decay of *URA3* mRNA was calculated from the fraction of full-length *URA3* mRNA remaining after various times in glucose (Fig. 2B). A half-life of 4–5 min was obtained, about half the value determined for genomic *URA3* mRNA in *S.cerevisiae* (31). Half-lives in this range yield values of 5–10 min between transcripts for normal levels (at steady-state) of *URA3* mRNA (see discussion in 15). This level of transcription is far lower than the number estimated for a single copy *GAL–URA–RIB* construct integrated into the *LEU2* locus of chromosome III (32). This difference most likely reflects both the high copy number of YRpSO1, measured to be ~50 copies/cell (data not shown), and insufficient amounts of Gal4 protein (Gal4p) in the cell (see Discussion). Indeed, the *GAL4* gene dosage limits transcription activation even in the small number of genomic galactose-inducible genes (33). Thus, we predict that few transcriptional events occur on a particular plasmid template during the repair incubation time (up to 4 h).

Chromatin structure of YRpSO1

To analyze the influence of nucleosomes on DNA repair in YRpSO1, as well as how the transcriptional status of the *GAL1:URA3* fusion gene affects its chromatin structure (32), we examined nucleosome positions in YRpSO1. For these studies, minichromosomes were partially purified, digested with micrococcal nuclease and the cutting sites mapped by indirect end-labeling from the *Asp*718 and *Xho*I sites, as well as from the *Eco*RI and *Sal*I sites (Fig. 1). The approximate positions are indicated in Figure 1 (small circles). We estimate that YRpSO1 has 22 nucleosomes generally distributed in four nucleosomal regions interrupted by four nuclease-sensitive gaps (Fig. 1).

The replication origin (*ARS1*) region is located in a nuclease-sensitive region flanked by a positioned nucleosome (Fig. 3). In addition, the nuclease-sensitive region includes the 3'-end of the *TRP1* gene (open arrowhead in Fig. 1) and the 3'-end of *URA3*. Although there is sufficient space for a nucleosome (Fig. 1, between nt 1531 and 1860), no footprint of a histone octamer is detected (see for example Fig. 3A, lanes 8–11, and B, lanes 1–4). The *HIS3* gene has five positioned nucleosomes and two nucleosomes are located on the *DED1* (Fig. 3B, lanes 8–11) and *PET56* elements (Fig. 3A, lanes 7–10), respectively. Nuclease-sensitive regions include the 5'-end of *DED1* and the 3'-end of *HIS3* and the 5'-ends of the *HIS3* and *PET56* sequences (Fig. 3). The upstream activation region of the *GAL1-10* promoter (or UAS_g) is located in a non-nucleosomal region (Fig. 1, small open rectangle) which is known to be insensitive to micrococcal nuclease (32,34). The *GAL1:URA3* fusion gene shows seven positioned nucleosomes.

Chromatin structures from cells grown in glucose and galactose media were similar throughout most of the minichromosome, including the region of the *GAL1:URA3* fusion gene. Clear differences in nucleosome arrangement were observed only in the *GAL3–GAL10* region (Fig. 3B, compare lanes 9 and 10). In glucose (D lanes), three positioned nucleosomes are observed

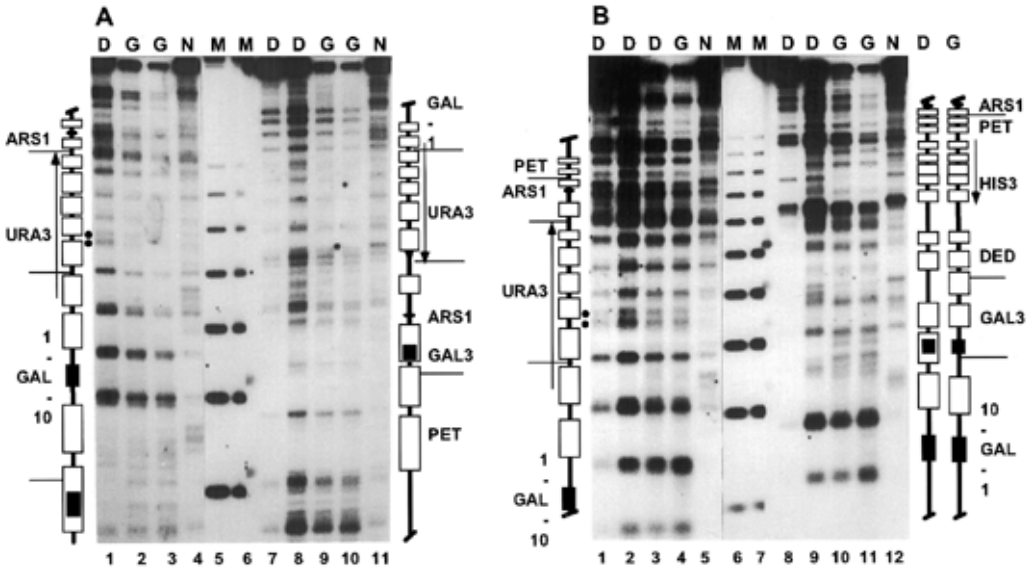

Figure 3. Chromatin analysis of YRpSO1 by micrococcal nuclease digestion and indirect end-labeling. Chromatin isolated from glucose-grown cells (D lanes) and galactose-grown cells (G lanes) and deproteinized DNA (N lanes) was digested with different amounts of micrococcal nuclease. A structural interpretation is shown on both sides of the gels. Protection regions of ~140–200 bp are interpreted as positioned nucleosomes (open boxes). Solid dots indicate a doublet of bands which may suggest a larger gap (or linker) betweeen nucleosomes or a lack of strong nucleosome positioning in that region. The marker (M) shows multiples of 256 bp from 1056 to 2560 bp (23). (**A**) Mapping of the cutting sites from the *Asp*718 (lanes 1–4) and the *Xho*I sites (lanes 7–11) (Fig. 1). (**B**) Mapping of the cutting sites from the *Eco*RI (lanes 1–5) and the *Sal*I sites (lanes 8–12) (Fig. 1). Schematic drawings to the right of the gel show the interpretation of structural changes between glucose- (D) and galactose-grown (G) cells.

in this region, as well as a nuclease-sensitive gap between those nucleosomes and the *DED1* nucleosomes. In galactose, two nucleosomes near the junction of *GAL3* and *GAL10* promoter are lost (or destabilized) and the nuclease-sensitive gap becomes protected from nuclease digestion (Fig. 3B, lanes 8–11).

The *GAL1:URA3* gene shows a regular series of bands with an average spacing of ~170 bp, consistent with a nucleosomal spacing. The pattern differs from the cutting sites observed in deproteinized DNA, indicating the influence of nucleosomes on nuclease accessability (compare N lanes with D and G lanes in Fig. 3). Clear differences between the N and D (or G) lanes are observed for the first three (after UAS_g) and the last two nucleosomes of *GAL1*:*URA3*, allowing one to infer that there are positioned nucleosomes in these regions. A doublet of bands at ~852 and 914 map units may suggest a larger gap (or linker) betweeen the third and forth nucleosomes or a lack of strong nucleosome positioning in that region (Fig. 3, solid dots). Surprisingly, no marked differences are observed in the chromatin organization of this region in cells grown in glucose and galactose (compare D and G lanes). However, when a similar construct is integrated as a single copy in the yeast genome, an altered nuclease digestion pattern, consistent with rearranged nucleosomes, is clearly observed (32). Since our chromatin analyses reflect the average status of the total minichromosome population, the similarity of the *GAL1:URA3* gene chromatin structure in glucose and galactose further indicates that only a minor fraction of the fusion genes are transcriptionally active at the time of harvest, in agreement with the transcription results (see above).

Overall repair of YRpSO1

The time course for repair of the YRpSO1 plasmid overall was determined by measuring the fraction of Form I molecules resistant to cutting by T4 endo V following different repair times (0–6 h). This enzyme specifically cleaves only the damaged strand of DNA at CPD sites (35) and the resulting fraction of Form I molecules (determined on neutral agarose gels) yields the average number of CPDs/plasmid assuming a Poisson distribution of damaged plasmids (24). The results indicate that when yeast cells are grown in galactose and irradiated at 30 J/m^2 (to yield an average of ~1 CPD/plasmid), the overall rate of repair in YRpSO1 is somewhat reduced compared with that in glucose and may reflect a slight decrease in UV survival in galactose-grown cells (data not shown). However, when cells were irradiated at a higher UV dose (100 J/m^2), which yields ~3 CPD/plasmid, the overall rate of repair in YRpSO1 was slightly increased in cells grown in galactose (Fig. 4). This result may reflect induced transcription of the *URA3* gene and/or other differences between yeast cells grown in these two different carbon sources.

Repair of CPDs at individual sites

Repair of CPDs was analyzed at 269 individual sites in three selected fragments of YRpSO1, which were chosen based on their proximities to the *GAL1:URA3* and *HIS3* genes (Fig. 1). The *GAL1–URA3* (*Dde*I–*Sty*I) fragment is located at the 5'-end

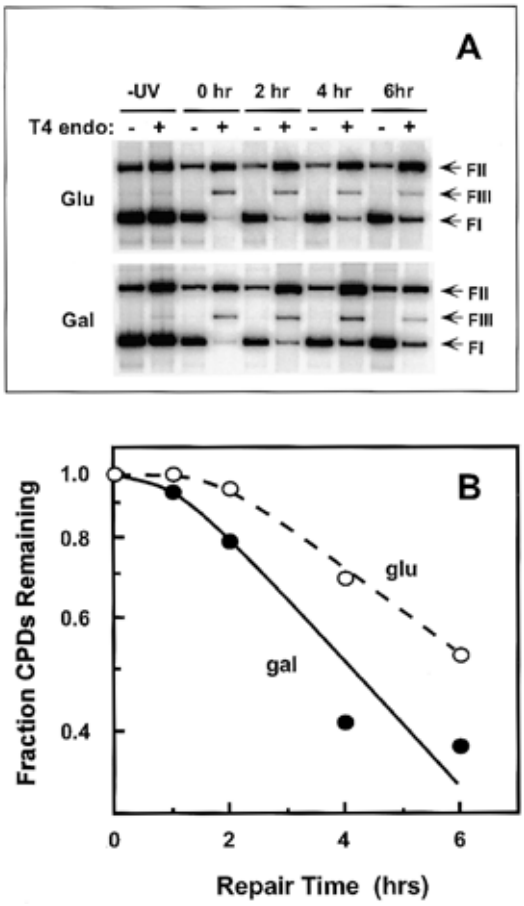

Figure 4. Whole plasmid repair of YRpSO1. (**A**) Representative blots of plasmid YRpSO1 from RGY1 cells that had been grown in glucose or galactose medium, irradiated with 100 J/m^2 UV and incubated for different repair times. Plasmid samples were either treated (+) or not treated (–) with T4 endo V, run on neutral agarose gels, transferred to nylon membranes, hybridized to probes generated from the whole plasmid of YRpSO1 and exposed to phosporimager screens. Note that following this UV dose, a significant amount of linear DNA (Form III) is present (due to T4 endo V cutting at multiple CPD sites/plasmid). (**B**) Fraction of CPDs repaired over time in the whole plasmid. Data were determined using all three bands [Forms I, II and III; see (A)] for the calculation of total intensity.

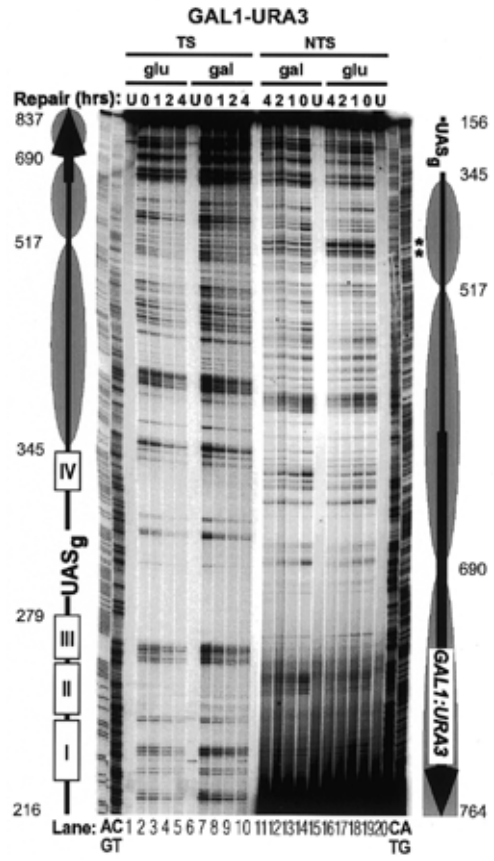

Figure 5. Phosphorimage of a sequencing gel showing the repair of CPDs at specific sites in the *GAL1–URA3* fragment. RGY1 cells were grown in minimal medium containing either glucose (glu) or galactose (gal), irradiated with 50 J/m^2 of UV light and allowed to repair for various times. Plasmid YRpSO1 was isolated, digested with *Dde*I and *Sty*I (to release the 678 bp *GAL1–URA3* fragment) and incised at CPD sites with an excess amount of T4 endo V. The T4 endo V-incised fragments were specifically end-labeled, resolved on DNA sequencing gels and exposed to phosphorimager screens. Lanes marked AG and CT are sequence markers generated via a modified procedure of Maxam–Gilbert sequencing. Schematic diagrams on each side show the interpreted structure of the minichromosome for this fragment, where the shaded ellipses denote the predicted nucleosome positions, the dark thick arrows denote the transcribed region and the open boxes with Roman numerals denote the GAL4p binding sites in the *UAS$_g$*. The stars denote CPD bands whose intensities were different between glucose and galactose cultures. The numbers on each side of the gel denote nucleotide positions clockwise from the unique *Eco*RI site of YRpSO1 (Fig. 1).

of the *GAL1:URA3* gene, which extends far into the *GAL1-10* promotor. The *URA3*–3' (*Stu*I) fragment is located at the 3'-end of the *URA3* gene, while the *HIS3* (*Bst*NI–*Bst*XI) fragment is at the 5'-end of the *HIS3* gene (Fig. 1).

Repair of CPDs was measured using a high resolution method developed by Li and Waters (26) for mapping CPDs at individual sites in a DNA fragment. This method uses streptavidin magnetic beads and biotinylated oligonucleotides to facilitate end-labeling of DNA fragments specifically incised at damage sites (25–27,36). After UV irradiation of yeast cells and different times of repair incubation, the plasmid molecules are isolated, digested with restriction enzymes and incised at the CPD sites with T4 endo V. The T4 endo V-incised fragments are specifically end-labeled, resolved on DNA sequencing gels and exposed to phosphorimager screens.

To ensure linearity of the individual CPD signals, a UV dose of 50 J/m^2 was used, which yielded 0.15–0.2 CPDs/single-stranded DNA fragment. At this dose, very few fragments contain more than one CPD, allowing for accurate quantitation of the CPDs remaining in each strand after different repair times. Figures 5 and 6 show representative phosphorimages of gels displaying the CPD sites in the three fragments. The pattern of CPD induction in the three analyzed fragments was

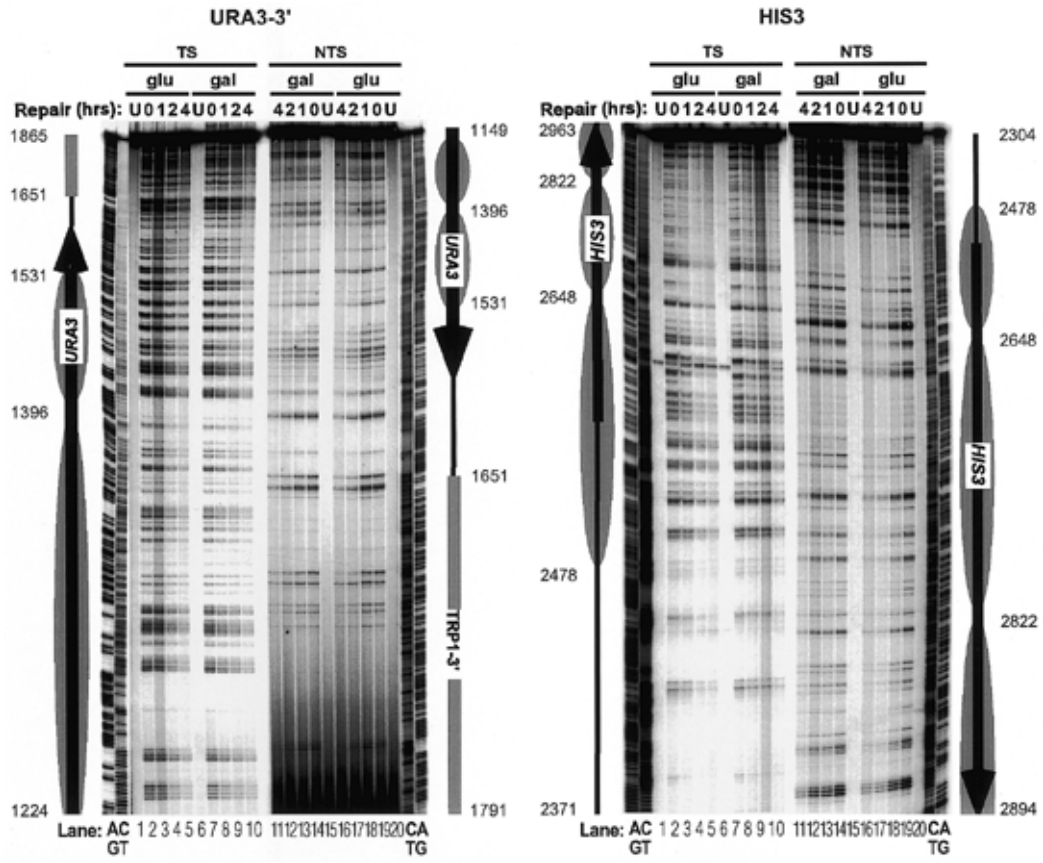

Figure 6. Phosphorimages of sequencing gels showing the repair of CPDs at specific sites in the *URA3*–3' and *HIS3* fragments. All treatments were the same as those described in the legend to Figure 5, except that *Stu*I and *Bst*NI–*Bst*XI were used to release the 717 bp *URA3*–3' and 659 bp *HIS3* fragments, respectively. Lanes marked AG and CT are sequence markers. Schematic diagrams on each side of the gels show the interpreted structure of the minichromosome for these fragments, where the shaded ellipses denote the predicted nucleosome positions and the dark thick arrows denote the transcribed regions. The shaded thick lines denote the 3'-end of the *TRP1* gene. The numbers on each side of the gels denote nucleotide positions clockwise from the unique *Eco*RI site of YRpSO1 (Fig. 1).

almost the same in glucose and galactose cultures, except for a few sites in the NTS of the *GAL1–URA3* fragment where induction is suppressed in galactose cultures (see bands marked with stars in the right half of Fig. 5). The UV 'photofootprints' were very similar to those reported by Axelrod *et al*. (37). However, the differences in CPD induction between the two cultures is much less striking in the minichromosome than in the genomic *GAL1-10* promoter (S.Li and M.Smerdon, unpublished observations). It is clear from these gels that CPDs are removed at most sites during the 4 h repair incubation (i.e. bands decrease in intensity).

Quantitation of the signals at each CPD site, using peak deconvolution analysis (25), yields the fraction of CPDs remaining after each repair time. Figure 7A shows an example of the CPDs remaining at the different sites in each fragment after 2 h repair incubation. In addition, Table 1 shows the averages of %CPDs remaining in both strands of the different regions. Faster repair occurred at many CPD sites in the TS of the *GAL1:URA3* fusion gene, including the *GAL1–URA3* and the *URA3*–3' fragments, when cells were switched from glucose (open circles) to galactose (solid triangles) medium. No significant difference was observed for the CPD sites in the NTS (Fig. 7A and Table 1). This faster repair was not restricted to the coding region of the TS in the induced *GAL1:URA3* fusion gene, but extended far upstream of the transcription start site (Fig. 7A and Table 1). Furthermore, although repair at most sites downstream of the transcription stop sequences in the TS of the *GAL1:URA3* fusion gene is slower than in the transcribed region, many of these sites are also repaired more rapidly when cells are grown in galactose medium (CPD sites between nt 1582 and 1808; Fig. 7A).

In contrast to the *GAL1:URA3* fusion gene, little difference is observed in repair of the TS of the *HIS3* gene between the two growth conditions (Fig. 7A). Presumably this observation reflects the lack of significant change in transcription of the *HIS3* gene (see above). [Interestingly, for unknown reasons, slower repair of CPDs occurs in the NTS upstream of the transcription start in *HIS3* in galactose cultures (Fig. 7A, between nt 2350 and 2520).] In both glucose and galactose cultures, faster repair occurs in the region immediately downstream of

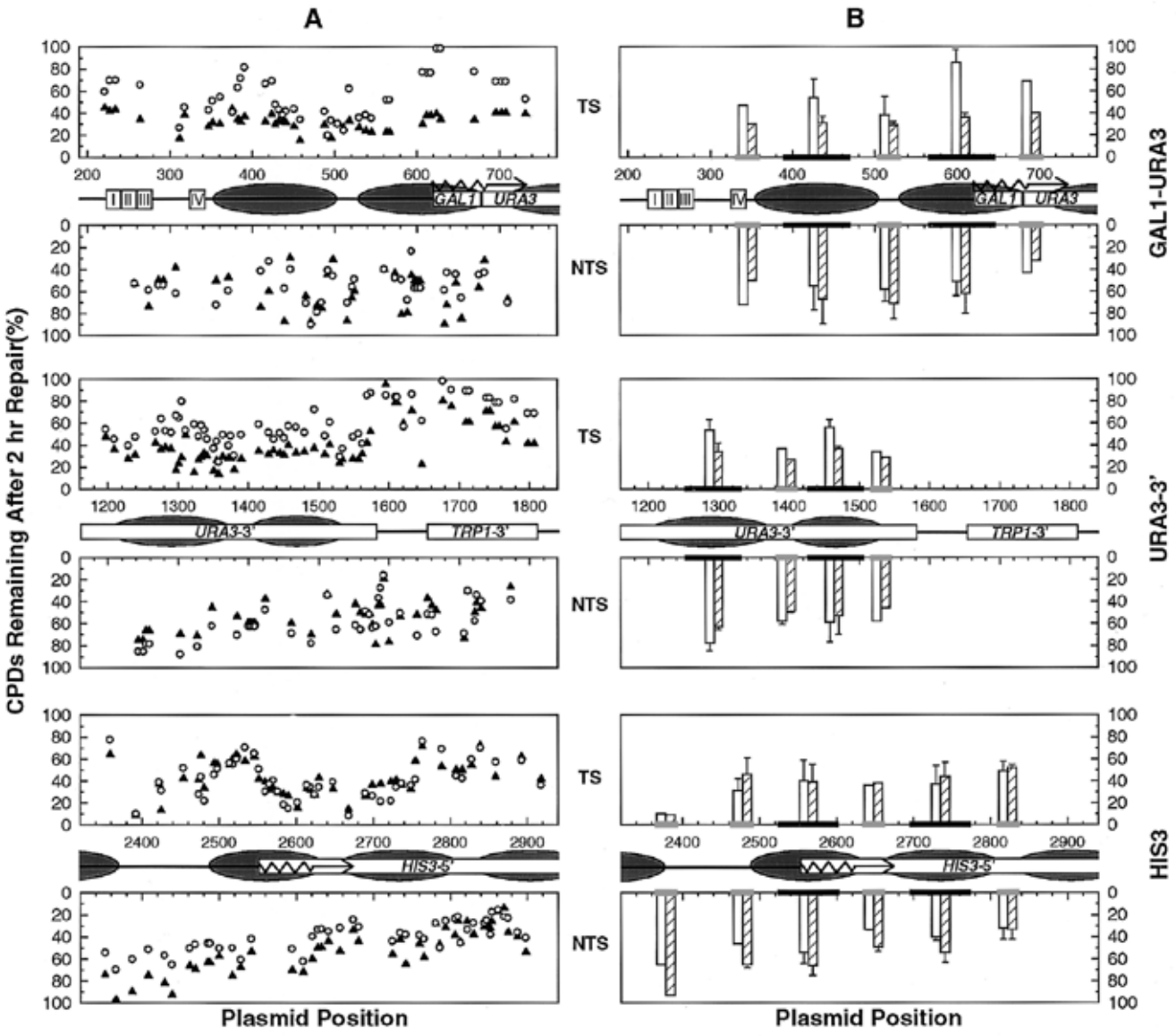

Figure 7. Percent CPDs remaining after 2 h of repair incubation in the *GAL1–URA3*, *URA3*–3' and *HIS3* fragments. (**A**) Data represent the %CPDs remaining at individual sites in glucose (open circles) or galactose (solid triangles) cultures. For each fragment, the top panel is for the TS and the bottom panel is for the NTS. Between the two panels a schematic diagram of the minichromosome region for each fragment is shown. The large shaded ellipses represent the approximate positions of nucleosomes, wavy arrows denote the major transcription start sites for the *GAL1:URA3* and *HIS3* genes and the open boxes with Roman numerals denote the Gal4p binding sites in the UAS_g. The numbering is clockwise from the unique *Eco*RI site of YRpSO1 (Fig. 1). (**B**) Averages of %CPDs remaining in the linker–core edge region (shaded horizontal bars) and interior core region (solid horizontal bars). Error bars, representing 1 SD, are shown only in the regions that contain three (or more) analyzed CPD sites. Symbols in the schematic diagrams are the same as those in (A). Open and hatched vertical bars denote glucose and galactose cultures, respectively. Values for the linker–core edge regions were calculated from segments of 30 nt centered at the strong micrococcal nuclease cut sites (Fig. 1). Values for the interior core regions were obtained from segments of 80 nt centered at the presumed nucleosome dyads.

the major transcription start site (between nt 2555 and 2750) of the *HIS3* gene (Fig. 7A). This differs from the pattern seen in the *GAL1:URA3* gene, in which fast repair was also observed in many sites upstream of the transcription start site when the gene is induced (Fig. 7A). However, repair is slower downstream of nt 2750 in the TS of the *HIS3* gene. When the %CPDs remaining at individual sites are averaged over the control or coding segments of the *HIS3* fragment, no significant difference is apparent between these two regions or between strands in the coding region (Table 1).

There is also a modest correlation between repair and presumed nucleosome positions in certain regions of YRpSO1 (Fig. 7A). In glucose cultures, relatively slow repair occurred in the TS of the *GAL1–URA3* fragment and in both strands of

Table 1. Repair of CPDs in different regions of YRpSO1

Fragment	Region[a]	Strand	%CPDs remaining after different repair times (h)[b]					
			Glu			Gal		
			1	2	4	1	2	4
GAL1–URA3	Control (nt 220–618)	TS	73 ± 12	51 ± 17	20 ± 8	58 ± 5	31 ± 8	22 ± 3
		NTS	74 ± 9	55 ± 14	39 ± 21	76 ± 12	58 ± 17	46 ± 13
	Coding (nt 619–733)	TS	90 ± 12	76 ± 17	35 ± 11	62 ± 2	38 ± 3	33 ± 4
		NTS	73 ± 8	53 ± 12	36 ± 12	81 ± 13	65 ± 20	42 ± 14
URA3–3'	Downstream–3' (nt 1582–1808)	TS	88 ± 9	81 ± 12	52 ± 15	84 ± 17	60 ± 15	32 ± 7
		NTS	73 ± 14	45 ± 16	20 ± 7	75 ± 15	41 ± 13	22 ± 9
	Coding (nt 1196–1581)	TS	76 ± 12	50 ± 13	23 ± 7	54 ± 9	34 ± 7	23 ± 8
		NTS	91 ± 9	62 ± 14	29 ± 12	86 ± 11	53 ± 12	22 ± 8
HIS3	Control (nt 2352–2555)	TS	72 ± 11	50 ± 16	25 ± 10	71 ± 10	50 ± 15	29 ± 9
		NTS	74 ± 6	54 ± 8	28 ± 5	87 ± 10	73 ± 13	44 ± 4
	Coding (nt 2556–2919)	TS	61 ± 15	37 ± 18	31 ± 18	63 ± 14	40 ± 16	38 ± 13
		NTS	61 ± 7	34 ± 11	15 ± 7	65 ± 10	42 ± 15	34 ± 10

[a]Nucleotide positions are clockwise from the unique *Eco*RI site of YRpSO1.
[b]Values (means ± 1 SD) for glucose (Glu) and galactose (Gal) cultures were calculated from all CPD sites in the respective regions.

the *URA3*–3' fragment, where nucleosomes are preferentially located. Conversely, relatively fast repair occurred in the linker regions (approximately centered at nt 517, 690, 1396 and 1531; Fig. 7A). In galactose cultures, this modest correlation was abolished in the TS of the fusion gene (Fig. 7A), indicating that the effect of transcription can override that of nucleosome positions on repair. Interestingly, little correlation was observed in the NTS of the *GAL1:URA3* or *HIS3* genes, irrespective of transcription (Fig. 7A). Averages (± 1 SD) of the %CPDs remaining in nucleosome 'linker–core edge' regions and 'interior core' regions are shown in Figure 7B. Segments of 30 and 80 nt were used for these regions, respectively, and demonstrate the modest correlation between CPD removal and nucleosome positioning (Fig. 7B). [We note that a 30 nt stretch was required for linker–core edge regions to obtain a minimum of one CPD site.]

DISCUSSION

We have examined the influence of transcriptional status and nucleosome positions on NER of UV-induced CPDs in a multicopy yeast minichromosome (YRpSO1) containing an inducible *GAL1:URA3* fusion gene, a constitutive *HIS3* gene and varied regions of chromatin structures (Fig. 1). Comparison of chromatin organization in YRpSO1 from cells grown in glucose and galactose showed no marked differences, except for the *GAL3–GAL10* region. The lack of change in chromatin structure of the promoter and the transcribed region of *GAL1:URA3* may reflect an insufficient amount of GAL4p in these cells. Indeed, Fedor and Kornberg (38) showed that the nucleosome structure and transcription of a high copy number minichromosome-borne *GAL1:URA3* fusion gene did not change appreciably if the cells did not contain an additional *GAL4* gene (supplied by a multicopy plasmid). Our estimation of the number of YRpSO1 molecules engaged in *active* transcription of the *GAL1:URA3* fusion gene at any one time supports this suggestion. Furthermore, we only observe a weak UV photofootprint in the NTS promoter region of the *GAL1–URA3* fragment upon galactose induction (Fig. 5). However, much more striking photofootprints are observed in this sequence in the single copy *GAL1-10* promoter in the genome (S.Li and M.Smerdon, unpublished results). Collectively, these findings indicate that only a small fraction of plasmids are undergoing transcription at any one time. As the technique we used for mapping nucleosome positions in YRpSO1 is colligative (i.e. represents an average of all the plasmids), it is not surprising that we see no perturbation of nucleosomes in this region.

We observed a clear difference in chromatin organization between glucose and galactose in the region where the *GAL3* upstream promoter elements are linked to the *GAL1-10* promoter (Fig. 1). However, no change was observed in the *DED1* sequence. It is therefore likely that factors interacting with UAS_g elements are involved in the structural reorganization when cells are shifted from glucose to galactose. Futhermore, although we did not detect an obvious change in nucleosome structure in the *GAL1:URA3* fusion gene upon galactose induction, we did observe a modulation of CPD yield at some sites in the promoter region of the fragment (see bands marked with stars in Fig. 5).

Using a 2.6 kb minichromosome, called TRURAP, we found that transcription-coupled repair correlates with the rate of transcription, except where two unstable nucleosomes reside (7,9,10). In the present study, preferential repair of CPDs was also observed in the transcribed strand of the *GAL1:URA3* fusion gene, but this strand preference was rather mild (Table 1). As mentioned above, this may reflect the fact that only a small fraction of plasmids are undergoing transcription at any one time.

These results raise the question of why do we observe transcription-coupled repair in the induced *GAL1:URA3* fusion gene at all, when so much of the plasmid population is transcriptionally silent? If we assume that only a few of the plasmid molecules are being actively transcribed at any time, our chromatin analysis will not observe much change between the two growth conditions. This will be the case regardless of when the cells are harvested. Similarily, immediately after UV irradiation only a few of the CPD sites will be in actively transcribing DNA. However, the repair rate depends on the frequency at which RNA polymerase II or NER encounters a lesion. In *GAL1:URA3*, transcription of the induced gene was enough to reveal preferential repair (Table 1). In contrast, there was no marked preferential repair (especially downstream of nt 2750; Fig. 7A) in the *HIS3* gene, indicating that transcription occurred very rarely in individual copies of this gene. We note that this logic also points to the need for a 'control gene' on the same plasmid where transcription changes little between the two growth conditions, as an internal reference to compare repair occuring in the inducible gene.

The 'start positions' for preferential repair (transcription-coupled repair) in different genes seem to vary and may also differ between bacteria and eukaryotes (27,36,39–44). It was originally proposed that this postion is downstream of the transcription start sites when RNA polymerase initiates elongation (39–42). More recently, however, it has been shown that preferential repair can occur immediately downstream (27,43) or even upstream (36,44) of the transcription start site. Furthermore, in yeast, fast repair immediately downstream of the transcription start site of the *RPB2* gene does not require the (putative) transcription–repair coupling factor Rad26 (43).

In the present study, we observed more rapid repair of CPDs in some sites far upstream of the transcription start site of the induced *GAL1:URA3* fusion gene (Fig. 7A). However, this was not observed in the constitutively expressed *HIS3* gene on the same plasmid, where some sites were repaired more rapidly and some sites more slowly (Fig. 7A). This observtion can be explained by a large fraction of inactive *HIS3* genes (i.e. larger than the inactive fraction of *GAL1:URA3* genes in the induced state). The fast repair upstream of the transcription start site of *GAL1:URA3* is probably not due to a stalled RNA polymerase at CPD sites, but rather results from either changes in local chromatin structure caused by transcription initiation or recruitment of repair factors by RNA polymerase at the initiation start site. Additionally, as some transcription initiation factors are also repair factors (reviewed in 6), enhanced repair at transcription start sites may result directly from transcription initiation.

For the NER apparatus to gain access to chromatin-packed DNA, at least some chromatin unfolding must occur (45). It is known that the rates of NER can vary widely within the genome and even within the same gene (see for example 39,46). Furthermore, CPDs in the NTS of the *URA3* gene in either a minichromosome or the genome of yeast are repaired most efficiently in linker DNA and towards the 5'-end of a positioned nucleosome and are repaired slower in the internal protected region of the nucleosome core (11,12).

In the present report, we analyzed NER of CPDs at 269 total sites in three fragments of YRpSO1 encompassing six nucleosomes. The results show a mild correlation between nucleosome positions and NER rates in the four nucleosomes of the *GAL1–URA3* and *URA3*–3' fragments. This correlation is strongest in the TS of the *GAL1–URA3* fragment when the fusion gene is not induced and is in general agreement with two previous reports on repair in this gene (11,12). Somewhat slower repair was also observed within nucleosomes approximately centered at nt 1293 and 1464 in the TS of the *URA3*–3' fragment (Fig. 7). However, no such correlation was observed in the NTS of the *GAL1–URA3* fragment in both growth conditions, even though heterogeneity of nucleosome positions is not strand selective. As mentioned above, the technique for nucleosome mapping of YRpSO1 measures a colligative property and the nucleosome positions (Fig. 1) we obtained are averages for the population. Indeed, we observed a more strict correlation between nucleosome positions and NER in both strands of the genomic *GAL1* gene (S.Li and M.Smerdon, unpublished results).

This study stresses some advantages and limitations of using minichromosomes as models for genomic repair. Analysis of repair in minichromosomes, with respect to chromatin structure and transcription, is appealing due to the much higher signals from multiple copies and restricted patterns of nucleosomes in these small DNAs. In this study, we observed transcription-coupled repair of CPDs in the induced *GAL1:URA3* fusion gene and not in the constitutive *HIS3* gene (regardless of carbon source) on the same plasmid. However, this coupling was not as dramatic as expected and may be limited by a lack of Gal4p required to induce transcription on all plasmid molecules (see above). Even with this limitation, however, it was apparent that the restricted correlation of NER with predicted nucleosome positions in the TS of uninduced *GAL1:URA3* was abolished upon induction of transcription. Furthermore, with constitutively expressed regions in another yeast minichromosome (TRURAP), we observed that nucleosomal instability may override the effect of transcription-coupled repair in a weakly expressed region (9).

ACKNOWLEDGEMENTS

We thank Dr Stephano Omari for construction of plasmid YRpSO1, Dr Jirair Bedoyan for contributing much of the earlier work characterizing YRpSO1, Dr R. Stephen Lloyd for supplying T4 endo V and Dr Louise Prakash for providing the yeast strain Y452. We also thank members of the Smerdon laboratory, particularly Drs James Mueller and Antonio Conconi, for technical help and critical discussions. This study was supported by NIH grant ES04106 from the National Institute of Environmental Health Sciences (M.J.S.) and by a grant from the Swiss National Science Foundation (F.T).

REFERENCES

1. Friedberg,E.C., Walker,G.C. and Siede,W. (1995) *DNA Repair and Mutagenesis*. ASM Press, Washington, DC.
2. Lehmann,A.R. (1998) *Bioessays*, **20**, 146–155.
3. Evan,G. and Littlewood,T. (1998) *Science*, **281**, 1317–1322.
4. Wood,R.D. (1996) *Annu. Rev. Biochem.*, **65**, 135–167.
5. Sancar,A. (1996) *Annu. Rev. Biochem.*, **65**, 43–81.
6. Friedberg,E.C. (1996) *Annu. Rev. Biochem.*, **65**, 15–42.
7. Smerdon,M.J. and Thoma,F. (1990) *Cell*, **61**, 675–684.
8. Sweder,K.S. and Hanawalt,P.C. (1992) *Proc. Natl Acad. Sci. USA*, **89**, 10696–10700.
9. Bedoyan,J., Gupta,R., Thoma,F. and Smerdon,M.J. (1992) *J. Biol. Chem.*, **267**, 5996–6005.

10. Smerdon,M.J., Gupta,R. and Murad,A.O. (1993) In Bohr,V.A., Wassermann K. and Kraemer,K.H. (eds), *DNA Repair Mechanisms, Alfred Benzon Symposium 35*. Munksgaard, Copenhagen, Denmark, pp. 258–270.
11. Wellinger,R.E. and Thoma,F. (1997) *EMBO J.*, **16**, 5046–5056.
12. Tijsterman,M., de Pril,R., Tasseron-de Jong,J.G. and Brouwer,J. (1999) *Mol. Cell. Biol.*, **19**, 934–940.
13. Omari,S. (1990) Chromatin structure during transcription in the yeast *Saccharomyces cerevisiae*, PhD thesis, Swiss Federal Institute of Technology, Zurich, Switzerland.
14. Johnston,M. and Davis,R.W. (1984) *Mol. Cell. Biol.*, **4**, 1440–1448.
15. Rose,M. and Botstein,D. (1983) *J. Mol. Biol.*, **170**, 883–904.
16. Rose,M., Grisafi,P. and Botstein,D. (1984) *Gene*, **29**, 113–124.
17. Thoma,F. and Simpson,R.T. (1985) *Nature*, **315**, 250–252.
18. Tschumper,G. and Carbon,J. (1980) *Gene*, **10**, 157–166.
19. Struhl,K. (1985) *Nucleic Acids Res.*, **13**, 8587–8601.
20. Ito,H., Fukuda,Y., Murata,K. and Kimura,A. (1983) *J. Bacteriol.*, **153**, 163–168.
21. Geitz,D.R. and Schiestl,R.H. (1991) *Yeast*, **7**, 253–263.
22. Ausubel,F.M., Brent,R., Kingston,R.E., Moore,D.D., Seidman,J.G., Smith,J.A. and Struhl,K. (1987) *Current Protocols in Molecular Biology*. John Wiley & Sons, New York, NY.
23. Thoma,F., Bergman,L.W. and Simpson,R.T. (1984) *J. Mol. Biol.*, **177**, 715–733.
24. Smerdon,M.J., Bedoyan,J. and Thoma,F. (1990) *Nucleic Acids Res.*, **18**, 2045–2051.
25. Li,S., Waters,R. and Smerdon,M.J. (1999) *Methods*, in press.
26. Li,S. and Waters,R. (1996) *Carcinogenesis*, **17**, 1549–1552.
27. Li,S. and Waters,R. (1997) *J. Mol. Biol.*, **271**, 31–36.
28. Sambrook,J., Fritsch,E.F. and Maniatis,T. (1989) *Molecular Cloning: A Laboratory Manual*, 2nd Edn. Cold Spring Harbor Laboratory Press, Cold Spring Harbor, NY.
29. Bajwa,W., Torchia,T.E. and Hopper,J.E. (1988) *Mol. Cell. Biol.*, **8**, 3439–3447.
30. Hargrove,J.L. and Schmidt,F.H. (1989) *FASEB J.*, **3**, 2360–2370.
31. Bach,M.L., Lacroute,F. and Botstein,D. (1979) *Proc. Natl Acad. Sci. USA*, **76**, 386–390.
32. Cavalli,G. and Thoma,F. (1993) *EMBO J.*, **12**, 4603–4613.
33. Johnston,S.A. and Hopper,J.E. (1982) *Proc. Natl Acad. Sci. USA*, **79**, 6971–6975.
34. Fedor,M.J., Lue,N.F. and Kornberg,R.D. (1988) *J. Mol. Biol.*, **204**, 109–127.
35. Dodson,M.L. and Lloyd,R.S. (1989) *Mutat. Res.*, **218**, 49–65.
36. Teng,Y., Li,S., Waters,R. and Reed,S.H. (1997) *J. Mol. Biol.*, **267**, 324–337.
37. Axelrod,J.D., Reagan,M.S. and Majors,J. (1993) *Genes Dev.*, **7**, 857–869.
38. Fedor,M.J. and Kornberg,R.D. (1989) *Mol. Cell. Biol.*, **9**, 1721–1732.
39. Gao,S., Drouin,R. and Holmquist,G.P. (1994) *Science*, **263**, 1438–1440.
40. Selby,C.P. and Sancar,A. (1994) *Microbiol. Rev.*, **58**, 317–329.
41. Kunala,S., and Brash,D.E. (1995) *J. Mol. Biol.*, **246**, 264–272.
42. Tijsterman,M., Tasseron-de Jong,J.G., van de Putte,P. and Brouwer,J. (1996) *Nucleic Acids Res.*, **24**, 3499–3506.
43. Tijsterman,M., Verhage,R.A., van de Putte,P., Tasseron-de Jong,J.G., and Brouwer,J. (1997) *Proc. Natl Acad. Sci. USA*, **94**, 8027–8032.
44. Tu,Y., Tornaletti,S. and Pfeifer,G.P. (1996) *EMBO J.*, **15**, 675–683.
45. Smerdon,M.J. and Thoma,F. (1998) In Nickoloff,J.A. and Hoekstra,M.F. (eds), *DNA Damage and Repair*, Vol. 2: *DNA Repair in Higher Eukaryotes*. Humana Press, Totowa, NJ, pp. 199–222.
46. Tornaletti,S. and Pfeifer,G.P. (1994) *Science*, **263**, 1436–1438.